Macromolecules

Article

pubs.acs.org/Macromolecules

Translational and Reorientational Dynamics of Entangled DNA

Zongying Gong and Johan R. C. van der Maarel*

Biophysics and Complex Fluids Group, Department of Physics, National University of Singapore, 2 Science Drive 3, Singapore 117551, Singapore

ABSTRACT: The end-group mean square displacement, molecular reorientation time, and radius of gyration of entangled λ-phage DNA molecules were measured with fluorescence microscopy. A frequency-dependent, complex diffusivity is derived by Fourier transformation of the mean square displacement. From a comparison of the diffusion moduli with the predictions of Doi–Edwards theory, the tube renewal time, step length, mean square end-to-end distance, Rouse relaxation time, and entanglement time are obtained. The reorientation time is derived from the orientation correlation of the radius of gyration tensor. The concentration dependencies of the tube renewal, reorientation, Rouse time, and entanglement time as well as the number of entanglements per DNA molecule agree with the relevant scaling laws for salted polyelectrolytes with screened electrostatics. Furthermore, the similarity in time scale for tube renewal and molecular reorientation brings into view the coupled translational and reorientational motion of DNA molecules in the entangled regime.

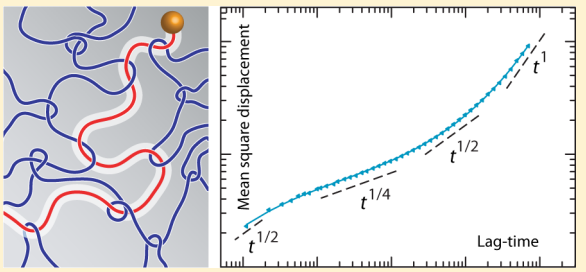

INTRODUCTION

The dynamical properties of DNA have an impact on many biological and biotechnological processes such as the replication of the genome and sizing in gel electrophoresis. At high concentration, DNA molecules tangle and form a dynamic network. The motion of a molecule is strongly hindered by topological constraints (entanglements) imposed by the presence of the other molecules. The dynamics of entangled DNA can be described by reptation theory.[1,2] This theory predicts that a linear molecule exhibits quasi one-dimensional diffusion within a virtual tube representing the constraints imposed by surrounding molecules. Reptation of entangled DNA has been shown by, among others, fluorescence microscopy imaging, diffusion, and microrheology experiments.[3−6] Furthermore, it has been shown that entanglements can be removed by a double strand passage reaction catalyzed by topoisomerase type II.[7,8]

One of the predictions of the reptation model is that the mean square displacement of polymer segments follows power laws in various regimes of the lag-time t according to

$$\langle \Delta r^2 \rangle \propto \begin{cases} t^{1/2} & t \lesssim \tau_e \\ t^{1/4} & \tau_e \lesssim t \lesssim \tau_R \\ t^{1/2} & \tau_R \lesssim t \lesssim \tau_d \\ t^{1} & \tau_d \ll t \end{cases} \quad (1)$$

Here, τ_e is the time required for the onset of the effect of tube constraints, τ_R is the Rouse time pertaining to the segmental motion within the tube, and τ_d is the longest translational relaxation time for tube renewal. Especially, the $\langle \Delta r^2 \rangle \propto t^{1/4}$ scaling related to the Rouse dynamics inside the tube is a hallmark of reptation. Because of the wide range of relaxation times, from milliseconds for τ_e to minutes for τ_d, the measurement of all four regimes in a single experiment for a unique sample has proven to be elusive. Reptation of flexible polymers has been investigated with computer simulation.[9−11] However, these studies mainly focus on the shorter lag-time dependence of the mean square displacement with $\langle \Delta r^2 \rangle \propto t^{1/4}$ scaling, because the relaxation times for tube renewal become prohibitively long for longer polymer chains.[12,13] Clear $t^{1/4}$ to $t^{1/2}$ and $t^{1/2}$ to t^1 transitions in the mean square displacement of polystyrene with increasing molecular weight have been observed with pulsed field gradient spin echo NMR.[14] NMR experiments have shown however that the transitions between the different regimes are gradual and that power law dependencies do generally not extend over a broad range in lag-times.[14,15]

We report the mean square displacement of quantum-dot end-labeled λ-phage DNA (48.5 kbp, contour length of 16.3 μm) as monitored by fluorescence microscopy. Our window of observation is such that we can observe the entire sequence of time scaling exponents in a single experiment. An innovative aspect is the derivation of the complex diffusivity based on the one-sided Fourier transformation of the mean square displacement of the end-group. The diffusion moduli will be interpreted in a similar way as the viscoelastic moduli, as obtained from microrheology with tracking of an embedded colloidal bead.[6,16−19] Note that diffusivity is not the same as viscoelasticity, despite the fact that they can be measured with a similar experimental methodology. A major difference

Received: August 6, 2014
Revised: September 22, 2014

   dx.doi.org/10.1021/ma501618a | *Macromolecules* XXXX, XXX, XXX–XXX

between a tagged DNA molecule and an embedded colloidal bead is that the DNA molecule exhibits internal relaxation modes. Accordingly, the diffusivity is sensitive to segmental motion besides viscoelastic dissipation in the surrounding fluid. From an analysis of the data at low frequencies, we will obtain the tube renewal time and the mean square end-to-end distance of the confinement tube. Information on the entanglement correlation length, number of entanglements per chain, entanglement time, and Rouse relaxation time for the motion of the entire DNA molecule inside the tube will be derived from an analysis of the diffusivity at higher frequencies. From fluorescence images of λ-DNA uniformly labeled with YOYO-1 dye, we will also obtain the radius of gyration of the entangled DNA molecules. The reorientation time of the DNA molecule will be derived from an analysis of the orientation correlation of the radius of gyration tensor.[20,21] The concentration scaling of the various parameters will be compared to the relevant theoretical predictions for polyelectrolytes with screened electrostatics.

THEORY

Summary of Reptation Theory. We have analyzed the mean square displacement of the end-group of λ-phage DNA with the reptation model originally proposed by de Gennes.[1] In the semidilute regime, there is full hydrodynamic interaction with nondraining conditions within the blobs of size ξ. Furthermore, at a sufficiently high concentration, the chain becomes entangled and partitioned into entanglement strands. The dynamics is Zimm-like up to the blob size ξ, Rouse-like for the strand of blobs between the entanglement points, and reptation-like for the entanglement strands. Here, the pertinent equations for the prediction of the motion are summarized using the notation of Doi and Edwards.[2] In this notation, the segment length b corresponds with blob size ξ and N denotes the number of blobs per chain. Since volume interactions are screened beyond ξ, the statistics of the Rouse chain of blobs is Gaussian with mean square end-to-end distance $R^2 = Nb^2$.

A test chain of N segments, each segment with length b, is thought to be confined to a temporal tube formed by entanglements with the other chains. The chain can only move along the primitive path with contour length L and step length a. The primitive path takes a Gaussian conformation with mean square end-to-end distance La. Note that the mean square end-to-end distance of the primitive path must be the same as that of the Rouse chain, so that $R^2 = La$. In the reptation model, there are three relaxation times, that is the time required for the onset of the effect of tube constraints τ_e, the Rouse time pertaining to the motion within the tube τ_R, and the longest relaxation time for tube renewal τ_d. The tube renewal time is related to the Rouse and entanglement time according to $\tau_d = 3Z\tau_R$ and $\tau_d = Z^3\tau_e/\pi^2$, respectively, with the number of entanglements per chain $Z = R^2/a^2$.

For times $t \gtrsim \tau_R$, the reptation dynamics of the primitive chain can be described by the Rouse model. The mean square displacement of the end segment is then given by[2]

$$\langle \Delta r^2(t) \rangle = \frac{2R^2}{\pi^2}\left[\frac{t}{\tau_d} + \sum_{p=1}^{\infty}\frac{2}{p^2}\left[1 - \exp\left(-\frac{p^2 t}{\tau_d}\right)\right]\right] \quad (2)$$

where we have replaced the $\cos^2(p\pi s/L)$ in the original expression for $\langle \Delta r^2 \rangle$ by unity because for the end-group the contour coordinate s equals zero or L. For very long lag-times $t \gg \tau_d$, self-diffusion is recovered, that is

$$\langle \Delta r^2(t) \rangle = \frac{2R^2}{\pi^2}\frac{t}{\tau_d} \quad (t \gg \tau_d) \quad (3)$$

On the other hand, for shorter times $\tau_R \lesssim t \lesssim \tau_d$, eq 2 takes the limiting form

$$\langle \Delta r^2(t) \rangle = \frac{4R^2}{\pi^{3/2}}\left(\frac{t}{\tau_d}\right)^{1/2} \quad (\tau_R \lesssim t \lesssim \tau_d) \quad (4)$$

In the Rouse model, the time dependence of $\langle \Delta r^2 \rangle$ is determined by the two parameters τ_d and R.

The Rouse model does not capture fluctuations for shorter times $t_e \lesssim t \lesssim \tau_R$. Once these fluctuations are included, the mean square displacement of the end-group takes the form[2]

$$\langle \Delta r^2(t) \rangle = \frac{4R}{\pi^{3/2}}\left[\frac{R^2 t}{\tau_d} + \sum_{p=1}^{\infty}\frac{2a^2}{3p^2}\left[1 - \exp\left(-\frac{p^2 t}{\tau_R}\right)\right]\right]^{1/2} \quad (5)$$

where the prefactor has been included to ensure a smooth transition to reptation dynamics for longer times in the range $\tau_R \lesssim t \lesssim \tau_d$ (eq 4). In the relevant range of times $\tau_e \lesssim t \lesssim \tau_R$, eq 5 takes the limiting form

$$\langle \Delta r^2(t) \rangle = \frac{4(2/3)^{1/2} a^{1/2} R^{3/2}}{\pi^{3/4}}\left(\frac{t}{\tau_d}\right)^{1/4} \quad (\tau_e \lesssim t \lesssim \tau_R) \quad (6)$$

Notice the characteristic $t^{1/4}$ scaling pertaining to the Rouse-like motion inside the tube. Furthermore, $\langle \Delta r^2 \rangle$ is now proportional to $a^{1/2}R^{3/2}$ and, hence, besides τ_d and R, sensitive to step length a.

For lag-times $t \lesssim \tau_e$, the segmental displacement is less than or comparable to a. The mean square displacement is then given by the short time limit of the Rouse model for an unconstrained chain[2]

$$\langle \Delta r^2(t) \rangle = a^2\left(\frac{t}{\tau_e}\right)^{1/2} \quad (t \lesssim \tau_e) \quad (7)$$

Notice the $t^{1/2}$ scaling and the dependence on a^2. For such short times, the mean square displacement is no longer dependent on R. For very short times $t \ll \tau_e$, the segment does not feel the constraints at all, so that $\langle \Delta r^2(t) \rangle \propto t$ pertaining to free diffusion is recovered.

Complex Diffusivity. We will find it convenient to analyze the motion of the end-segment in the frequency rather than time domain. In analogy with the definition of the viscous loss and elastic storage moduli,[18] we define a complex diffusivity

$$M(i\omega) = M'(\omega) + iM''(\omega) = [i\omega\langle \Delta\tilde{r}^2(i\omega)\rangle]^{-1} \quad (8)$$

with the one-sided, complex Fourier transform of the mean square displacement

$$\langle \Delta\tilde{r}^2(i\omega)\rangle = \int_0^{\infty} \mathrm{d}t\, \exp(-i\omega t)\langle \Delta r^2(t)\rangle \quad (9)$$

and real frequency ω. The complex diffusivity $M(i\omega)$ is related to the frequency dependent diffusion constant $D(i\omega)$, as being the one-sided Fourier transform of the velocity correlation function, according to

dx.doi.org/10.1021/ma501618a | Macromolecules XXXX, XXX, XXX−XXX

$$M(i\omega) = i\omega/(6D(i\omega)) \tag{10}$$

Note that $M(i\omega)$ is not the same as the complex viscoelasticity modulus $G(i\omega)$. The latter modulus can be determined by, for instance, a microrheology experiment with tracking of an embedded colloidal bead with a size larger than the structures of the fluid. A tagged DNA molecule can be considered as such a probe particle, but a major difference is that it also exhibits internal relaxation modes. Accordingly, $M(i\omega)$ is sensitive to segmental dynamics (reptation and Rouse) besides viscoelastic response of the surrounding fluid.

The diffusion moduli pertaining to reptation dynamics are readily calculated by transforming eq 2, that is

$$M^{-1}(i\omega) = \frac{2R^2}{\pi^2}\left[\frac{1}{i\omega\tau_d} + \sum_{p=1}^{\infty}\frac{2}{i\omega\tau_d + p^2}\right] \tag{11}$$

which takes the limiting forms

$$M'(\omega) = \frac{\pi^4(\omega\tau_d)^2}{6R^2}, \quad M''(\omega) = \frac{\pi^2\omega\tau_d}{2R^2} \quad (\omega \ll \tau_d^{-1}) \tag{12}$$

and

$$M'(\omega) = M''(\omega) = \frac{\pi(\omega\tau_d)^{1/2}}{2^{3/2}R^2} \quad (\tau_d^{-1} \lesssim \omega \lesssim \tau_R^{-1}) \tag{13}$$

for lower and higher frequencies, respectively. Limiting expressions of the diffusion moduli in the Rouse and high frequency regimes are obtained by transforming eqs 6 and 7, that is

$$M'(\omega) = \frac{(3/2)^{1/2}\pi^{3/4}\cos(\pi/8)(\omega\tau_d)^{1/4}}{\Gamma(1/4)a^{1/2}R^{3/2}}$$

$$M''(\omega) = \frac{(3/2)^{1/2}\pi^{3/4}\sin(\pi/8)(\omega\tau_d)^{1/4}}{\Gamma(1/4)a^{1/2}R^{3/2}}$$

$$(\tau_R^{-1} \lesssim \omega \lesssim \tau_e^{-1}) \tag{14}$$

and

$$M'(\omega) = M''(\omega) = \frac{(2/\pi)^{1/2}(\omega\tau_e)^{1/2}}{a^2} \quad (\omega \gtrsim \tau_e^{-1}) \tag{15}$$

respectively.

Notice that a transition through $t^{1/2}$ scaling of the mean square displacement results in a crossover of the moduli with $M' = M''$ at the crossover frequency (see eqs 13 and 15). For entangled solutions, there are two crossover frequencies: one at a relatively low frequency $\omega \approx \tau_d^{-1}$ and another one at a high frequency $\omega \approx \tau_e^{-1}$. We will determine R and τ_d from a fit of eq 11 to the experimental data in the low frequency range $\omega \lesssim \tau_d^{-1}$. Step length a will be determined from the values of the moduli in the intermediate range of frequencies pertaining to $\omega^{1/4}$ scaling, that is in the range $\tau_R^{-1} \lesssim \omega \lesssim \tau_e^{-1}$, or at the high frequency crossover point $\omega \approx \tau_e^{-1}$.

EXPERIMENTAL PROCEDURES

Sample Preparation. Bacteria λ-phage DNA was purchased from New England Biolabs, Ipswich, MA and used without further purification. Single stranded oligonucleotide with the complementary base pair sequence 5′-GGTCGCCGCCC-3′ to the right cohesive end of λ-phage DNA was purchased from Sigma-Aldrich, St. Louis, MO. As received from the manufacturer the λ-phage DNA stock solution has a concentration of 0.5 g of DNA/L. The solvent is TE buffer, which is composed of 10 mM Tris−HCl, pH 8.0, and 1 mM EDTA. Water was deionized and purified by a Millipore system and has a conductivity less than 1×10^{-6} $\Omega^{-1}\text{cm}^{-1}$. The DNA stock solution was concentrated to a concentration of 2.2 g of DNA/L with a Amicon centrifugal filter unit (Millipore, 30 kDa cutoff). The DNA concentration of the stock solution was determined by UV spectrometry. In order to remove naturally formed concatemers, the stock solution was heated to 338 K for 10 min, then rapidly cooled to 295 K by immersion in a water bath, and the complementary oligonucleotide was subsequently hybridized to one of the overhangs with a molar ratio of one DNA molecule to 25 oligonucleotides.

Quantum dot 565 streptavidin conjugate was purchased from Invitrogen, Carlsbad, CA. Biotinylated 5′-GGTCGCCGCCC-3′ oligonucleotide was purchased from Integrated DNA Technology, Coralville, IA. T4−DNA ligase and T4 ligase reaction buffer were obtained from New England Biolabs. For quantum dot end labeling, 20 μL of 0.5 g λ-phage DNA/L was diluted to 180 μL, then heated to 338 K for 10 min, and subsequently mixed with 300 pmol of biotin modified oligonucleotide in 1× T4−DNA ligase reaction buffer to a final volume of 290 μL. After overnight incubation at room temperature, 10 μL of T4−DNA ligase was added to the solution and incubated at room temperature for 2 h. The ligation reaction was stopped by heating to 338 K for 20 min, followed by washing of the ligated DNA (3 times) with TE buffer using the above-mentioned centrifugal filter units with 100 kDa cut off. Quantum dot 565 streptavidin conjugates were subsequently added at a dot per DNA ratio of 5:1 in the presence of 50 mM NaCl. After incubation at room temperature for 2 days, excess, nonbound quantum dots were removed by centrifugation.

For the measurement of the displacement, a part of the stock solution was spiked with quantum dot end-labeled DNA. For the determination of the radius of gyration as well as the reorientational relaxation time, a small amount of YOYO-1 labeled DNA with an intercalation ratio of 15 base-pairs per dye molecule was added to another part of the stock solution. The stocks have a final concentration of 0.125 mg of labeled DNA/L (the total DNA concentration is 2.2 g/L). Series of samples with DNA concentrations in the range 0.2−1.5 g/L was subsequently prepared by dilution of the stock solutions with TE buffer. The final solutions were subsequently equilibrated for at least 48 h in a controlled humidity chamber at 277 K. In order to minimize photobleaching of the YOYO−1 dye, β-mercaptoethanol (4%(v/v), Sigma-Aldrich) was added to the corresponding samples 1 h before imaging. For each experiment, a droplet of solution was deposited on a microscopy slide and sealed with a coverslip separated by a 0.12 mm spacer.

End-Segment Tracking. DNA tracking experiments were done at ambient temperature (296 K) with a Nikon Eclipse Ti microscope equipped with a 200 W metal halide lamp, a filter set, and a 100× oil immersion objective. The height level of the focal plane was adjusted so that it is situated midway between slide and coverslip. Video was collected with an electron multiplying charge coupled device (EMCCD) camera (Andor iXon X3) and Andor Solis software. We have checked our setup by measuring the diffusion of colloidal beads dispersed in a concentrated solution of glycerol as well as by monitoring immobilized beads adsorbed at a glass slide. A series of video clips was recorded with a rate of 90 frames per second, full frame size of 128 × 128 pixels and exposure time of 9 ms. The exposure time is short enough to minimize dynamic error and the static error in $\langle\Delta x^2\rangle$, as estimated by monitoring immobilized beads, is around 10 nm.[20] Each clip has duration of 5 min and the total duration of the movie is 200 min. The clips were taken randomly in the xy plane and in each clip the trajectories of one to two DNA molecules were recorded. Accordingly, 40 to 80 different DNA molecules constitute each ensemble averaged mean square displacement, but the maximum lag-time is 100 s. The video was analyzed with matlab (Natick, MA) and the DNA trajectories were obtained with public domain tracking software.[28] All further data analysis was done with home-developed

dx.doi.org/10.1021/ma501618a | Macromolecules XXXX, XXX, XXX−XXX

software scripts written in matlab code.[6,7] The pixel size in the x and y directions of 0.16 μm was determined with a metric ruler.

Reorientation. The reorientation correlation time was determined by tracking of YOYO-1 labeled DNA.[21] The methodology is similar to the one pertaining to the tracking of the translational motion of end-labeled DNA as described above. Here, the duration of each video clip is 3 min and the total duration of the movie is 120 min. In order to increase the signal-to-noise ratio, the frame rate was reduced to 45 frames per second. With one or two imaged DNA molecules per clip, 40 to 80 different DNA molecules constitute the ensemble from which the radius of gyration and reorientation correlation time are derived. For each frame (time t), the radius of gyration tensor was constructed according to

$$\mathbf{S}(t) = \frac{1}{I_0}\sum_{m,n}(\mathbf{r}_{mn} - \mathbf{r}_{cm})^2 I_{mn} \tag{16}$$

with I_{mn} the fluorescence intensity of pixel $[m,n]$ at position $\mathbf{r}_{mn}$ in the xy-plane and I_0 the total intensity of the frame. The center of mass $\mathbf{r}_{cm}$ of the molecule was calculated according to

$$\mathbf{r}_{cm} = \frac{1}{I_0}\sum_{m,n}\mathbf{r}_{mn} I_{mn} \tag{17}$$

The time-dependent $\mathbf{S}$ carries information about the instantaneous size, shape, and orientation of the DNA molecule. For each frame, we determined the principal eigenvalues and vectors of $\mathbf{S}$ using a singular value decomposition and with the assumption of cylindrical symmetry. The eigenvalues of $\mathbf{S}$, that is $S_\parallel$ and $S_\perp$, represent the length of the long and short axis, respectively. We derived the radius of gyration according to

$$R_g = \frac{1}{2}\langle (S_\parallel^2 + S_\perp^2)^{1/2}\rangle \tag{18}$$

where the brackets denote an average over all frames.

The instantaneous orientation of the radius of gyration tensor was obtained from the angle enclosed by the principal eigenvector and the x-axis using

$$\theta = \arctan\left(\frac{S_\parallel - S_{xx}}{S_{xy}}\right), \quad -\frac{\pi}{2} \le \theta \le \frac{\pi}{2} \tag{19}$$

In order to derive information about reorientational dynamics, we constructed the time autocorrelation function of the angle θ according to

$$C(\tau) = \frac{\langle \theta(t)\theta(t-\tau)\rangle}{\langle \theta^2\rangle} \tag{20}$$

where the brackets denote an ensemble average (average over all frames with different times t). As will be shown shortly, the autocorrelation function decays exponentially

$$C(\tau) = \exp(-2\tau/\tau_r) \tag{21}$$

with reorientation time τ_r. The factor of 2 in the exponential decay is due to the fact that the angle θ covers half of the phase space ($-\pi/2 \le \theta \le \pi/2$).

RESULTS AND DISCUSSION

Mean Square Displacement. From the trajectories of the quantum dots attached to the end of λ-phage DNA, the probability distributions for end-segment displacements in the x and y directions were extracted for a range of lag-times t. The minimum lag-time of 9 ms is determined by the frame rate of the camera. The practical limit of the maximum lag-time is 100 s, for longer times the quantum dots lose their intensity due to photobleaching and/or the molecules are subjected to long time coherent flow. An example of the probability distributions for the displacements in the two orthogonal directions is shown in Figure 1. A Gaussian was fitted to both probability distributions by optimizing the mean square displacements.

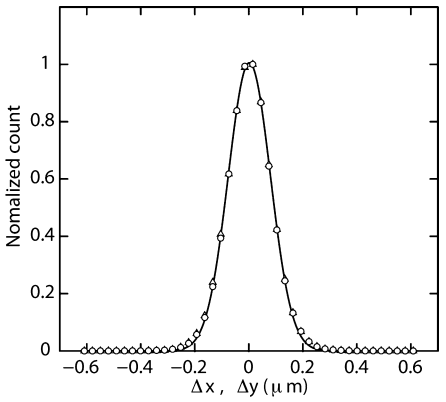

Figure 1. Probability distribution for the displacement Δx (Δ) and Δy ($\bigcirc$) of end-labeled λ-phage DNA for lag-time t = 1.155 s. The DNA concentration is 0.9 g/L. The symbols denote the data, whereas the solid curve represents a Gaussian fit. Data pertaining to both directions overlap within experimental error.

Irrespective lag-time, the mean square displacements in the x and y directions are equal within experimental error, and we henceforth report the average value. The results pertaining to a range in concentrations from 0.2 to 1.5 g of DNA/L are displayed in Figure 2. We use the symbol $\langle \Delta x^2\rangle$ to stress that

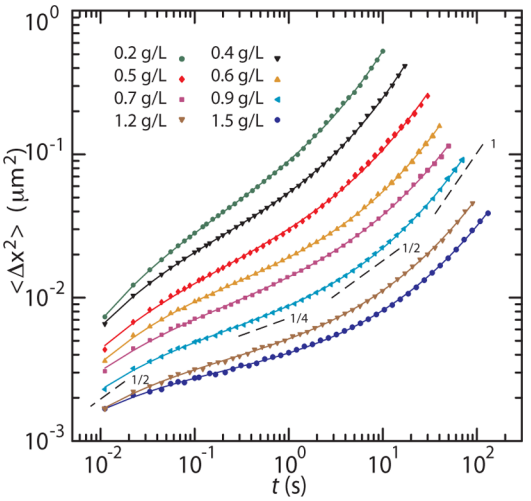

Figure 2. Mean square displacement $\langle \Delta x^2\rangle$ of end-labeled λ-phage DNA versus lag-time t. The dashed lines represent power laws with noted exponents. Notice the change in exponent from 1/2 through 1/4, 1/2, to 1 with increasing lag-time for a concentration of 0.9 g of DNA/L.

we are referring to the mean square displacement in one dimension; albeit, the experimental results are obtained by statistically averaging the widths of the distributions obtained in the x and y directions.

In the double logarithmic representation and with increasing lag-time, $\langle \Delta x^2\rangle$ first increases, then levels off to a certain extent depending on the DNA concentration, and eventually increases again. Diffusive behavior with $\langle \Delta x^2\rangle \propto t$ is recovered for very long times exceeding 10 to 100 s, depending on the concentration of DNA. For shorter times, deviations from diffusive behavior with scaling exponents less than one are

dx.doi.org/10.1021/ma501618a | Macromolecules XXXX, XXX, XXX−XXX

observed. With increasing DNA concentration, $\langle \Delta x^2 \rangle$ decreases and the range of times with subdiffusive scaling exponents becomes wider. Similar behavior has been reported before for the displacement of micron-sized colloidal beads immersed in otherwise the same solutions of λ-phage DNA. The deviation from diffusive behavior is attributed to the formation of entanglements for concentrations exceeding 0.3 g of DNA/L.[6] These phenomena are more conveniently discussed in terms of the diffusion moduli to be presented below.

The change in scaling exponent is illustrated in a plot of the first order derivative $\partial[\log\langle \Delta x^2(t) \rangle]/\partial[\log t]$ versus lag-time t. An example of such a plot pertaining to a concentration of 0.9 g of DNA/L is shown in Figure 3. With increasing lag-time, the

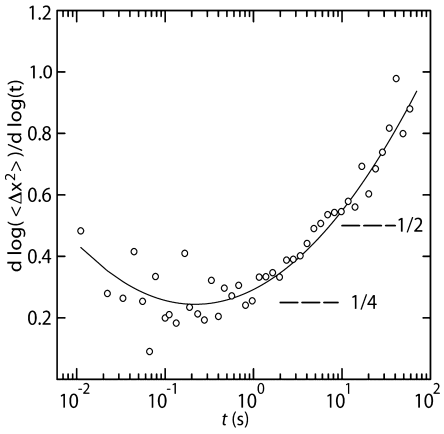

Figure 3. Time scaling exponent of the mean square displacement of end-labeled λ-phage DNA. The concentration is 0.9 g of DNA/L. The circles are the experimental data, whereas the solid curve represents a second order polynomial fit.

scaling exponent initially decreases from a value of around 1/2 to 1/4. This initial decrease reveals the onset of tube constraints. A scaling exponent of 1/4 is due to the Rouse dynamics inside the tube and is a hallmark of reptation. For longer times, the scaling exponent increases again through a value of 1/2 due to the reptation of the primitive path, and, eventually, it reaches the value of unity pertaining to diffusion. To the best of our knowledge, this is the first observation of the change in time scaling through the complete sequence $t^{1/2}$, $t^{1/4}$, $t^{1/2}$, t with increasing displacement time for a unique sample in a single experiment. Notice however that the scaling exponent changes gradually and even becomes smaller than 1/4 for concentrations exceeding 0.9 g of DNA/L.

The fact that the system is characterized by multiple length and time scales is illustrated in Figure 4. Here, the mean square displacement has been normalized to the mean square end-to-end distance R^2 and the lag-time has been divided by the longest relaxation time for tube renewal τ_d (R and τ_d were obtained from a fit of the predictions of the Rouse model, see below). For longer scaled lag-times $t/\tau_d > 1$, the normalized curves pertaining to different concentrations of DNA collapse to a single master curve. Diffusive behavior with an exponent of unity is observed for lag-times exceeding tens of the tube renewal time. For $t/\tau_d < 1$, the individual normalized curves deviate from each other due to concentration dependent differences in the extent to which the molecules are tangled (different entanglement times, Rouse times, and step lengths).

Diffusion Moduli. The diffusion moduli M' and M'' were calculated from the mean square displacement according to eq

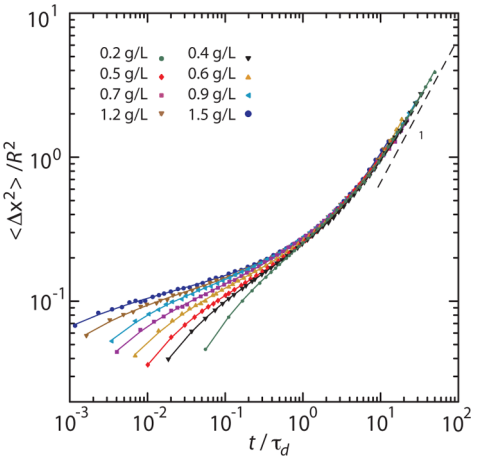

Figure 4. Mean square displacement normalized to the mean square end-to-end distance $\langle \Delta x^2 \rangle/R^2$ versus lag-time normalized to the longest relaxation time for tube renewal t/τ_d. Notice the converge of the data pertaining to various concentrations of DNA to a single master curve for $t/\tau_d > 1$.

8 using a fourth order polynomial fit as described in ref 6. The polynomial fits are also shown in Figure 2 and they describe the smooth variation of the mean square displacements well. The resulting moduli are displayed in Figure 5 for a representative set of concentrations. The results for the other concentrations fall perfectly between the marks set by the 0.2, 0.5, 0.9, and 1.5 g of DNA/L solutions and are not shown. Qualitatively, the diffusion moduli exhibit the same frequency dependent behavior as the viscoelasticity moduli obtained by tracking of an embedded colloidal bead in otherwise the same solutions of DNA.[6]

With increasing frequency, M'' first increases, then levels off or even decreases a bit, and eventually increases again. Concurrently, M' monotonously increases and eventually levels off, but does not reach a plateau value within our window of observation (except for the lowest concentration of 0.2 g of DNA/L). With increasing concentration, M' becomes increasingly larger than M'' in an intermediate frequency range. The crossing of the moduli is related to the formation of entanglements for concentrations exceeding 0.3 g of DNA/L. Similar entanglement concentrations were estimated before from self-diffusion (in the limit of long lag-times) and viscoelasticity experiments.[5,6] The concentrations are at least an order of magnitude higher than the overlap concentration from the dilute to the semidilute regime. Note that the crossover frequencies correspond to inverse lag-times for which the mean square displacement scales as $t^{1/2}$ (see eqs 13 and 15). The lowest crossover is related to the tube renewal or disengagement time and occurs at $\omega\tau_d \approx 1$. With increasing concentration, τ_d increases and, hence, the corresponding crossover frequency decreases. The high-frequency crossover is determined by the entanglement time according to $\omega\tau_e \approx 1$. With increasing concentration, the entanglement time decreases and the corresponding crossover frequency increases. Unfortunately, due to the limited frame rate of our camera, the highest crossover frequency shifts outside the window of observation for concentrations exceeding 0.7 g of DNA/L. The values of the moduli at the lowest and highest crossover frequencies are inversely proportional to the mean square end-to-end distance R^2 and step length a^2, respectively.

dx.doi.org/10.1021/ma501618a | Macromolecules XXXX, XXX, XXX–XXX

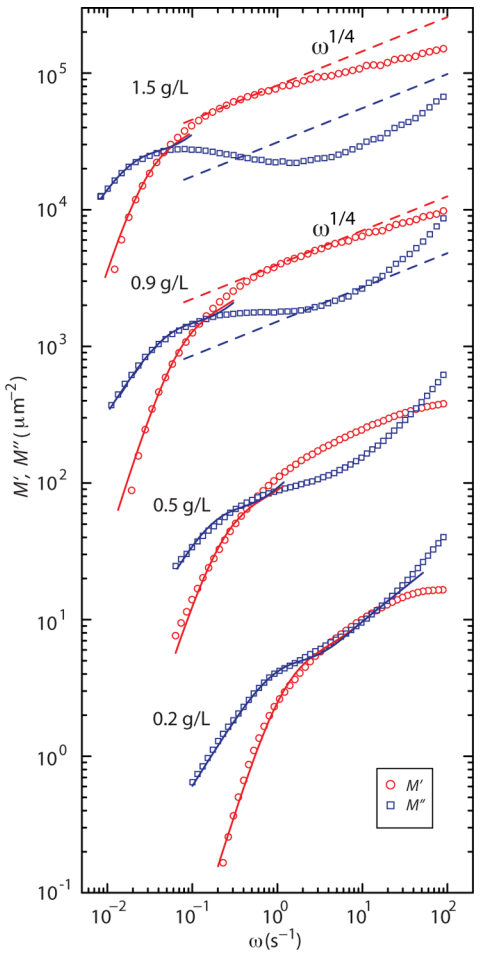

Figure 5. (A) Diffusion moduli M' (red ○) and M'' (blue □) versus frequency ω for the noted concentrations of DNA. The solid lines represent the Rouse diffusion model in the range $\omega \lesssim \tau_d^{-1}$. The dashed lines denote M' (red) and M'' (blue) pertaining to Rouse dynamics inside the tube (for $c > 0.7$ g/L). The moduli are shifted along the z-axis with a multiplicative factor of a power of 10 to avoid overlap.

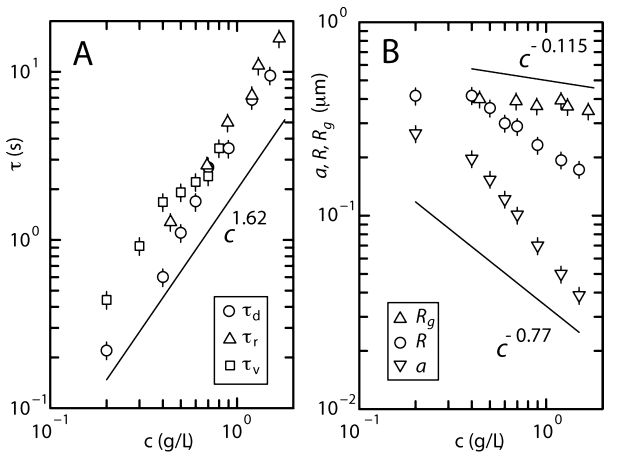

Figure 6. (A) Tube renewal time τ_d (○), viscoelastic relaxation time τ_v (□), and reorientation time τ_r (Δ) versus DNA concentration c. (B) As in panel A, but for the radius of gyration R_g (Δ), end-to-end distance R (○), and step length a (▽). The solid lines represent the scalings law of the longest relaxation time $\tau \simeq c^{1.62}$, radius of gyration $R_g \simeq c^{-0.115}$, and step length $a \simeq c^{-0.77}$.

Reptation dynamics of the DNA molecules in the entangled solutions is revealed at the lowest frequencies with $\omega \lesssim \tau_d^{-1}$. The dispersion observed at higher frequencies is related to Rouse dynamics of the entire DNA molecule inside the tube formed by the entanglements. Quantitative information on the number of entanglements per chain and the Rouse relaxation time will be obtained below from a comparison of the moduli to some of the predictions of Doi–Edwards theory. We will first focus on reptation dynamics, which will be analyzed with the Rouse model in its simplest form.

Reptation Dynamics. The tube renewal time τ_d and the mean square end-to-end distance R^2 can be determined from a fit of the predictions of the Rouse model in eq 11 to the experimental diffusion moduli in the relevant range of frequencies. As can be seen in Figure 5, excellent agreement between the data and theoretical prediction is observed up to and including the lowest crossover frequency $\omega \lesssim \tau_d^{-1}$. For higher frequencies, the Rouse model in its simplest form is not applicable and does not give a satisfactory agreement with the data. In the limit $\omega \ll \tau_d^{-1}$, M' and M'' approaches ω^2 and ω scaling as predicted by eq 12. The fitted values of τ_d and R are displayed in Figure 6, parts A and B, respectively.

The tube renewal time τ_d increases by an order of magnitude from 0.2 to 10 s when the concentration is increased from 0.2 to 1.5 g of DNA/L. For comparison, we have also included in Figure 6A the longest relaxation time pertaining to viscoelasticity τ_v, as obtained from previously reported microrheology experiments.[6] Although the latter relaxation times were determined for a slightly less extended range of concentrations of DNA, τ_d and τ_v are in reasonable agreement and follow the scaling law for reptation dynamics of polyelectrolytes with screened electrostatcs $\tau \simeq c^{1.62}$ (Flory exponent $(3-3\nu)/(3\nu - 1)$ with $\nu = 0.588$).[22−24]

The concentration dependence of the fitted end-to-end distance R is shown in Figure 6B. For comparison, we have also included the radius of gyration of the DNA molecule R_g as obtained from fluorescence imaging of YOYO-1 labeled DNA (see below). The radius of gyration is around 0.4 μm and slightly decreases with increasing concentration according to the relevant scaling law for polyelectrolytes with screened electrostatics in the semidilute regime $R_g \simeq c^{-0.115}$ (Flory exponent $(1 - 2\nu)/(6\nu - 2)$ with $\nu = 0.588$).[22−26] The fitted values of the end-to-end distance R show a steeper decrease from 0.40 to 0.18 μm if the concentration is increased from 0.2 to 1.5 g of DNA/L. Furthermore, the values of R appear to be somewhat underestimated (and/or R_g overestimated), because for a Gaussian chain $R = (6)^{1/2}R_g$. The discrepancies between R and R_g might be related to unaccounted effects in the present implementation of the Doi–Edwards model such as fluctuations of the length of the primitive path and primitive path reorganization by constraint release and tube deformation.[2]

Rouse Dynamics. The behavior of the moduli at higher frequencies is related to Rouse dynamics of the entire DNA molecule inside the tube. A second, high frequency crossover is observed at $\omega \approx \tau_e^{-1}$ for samples up to and including a concentration of 0.7 g of DNA/L. Step length a can then be determined from the inverse of the values of the moduli at the crossover point according to eq 15. For concentrations exceeding 0.7 g of DNA/L, the crossover shifts outside our window of observation. However, the latter solutions are well entangled (see below) and the mean square displacement exhibits $t^{1/4}$ scaling for certain lag-times. This is best illustrated

dx.doi.org/10.1021/ma501618a | Macromolecules XXXX, XXX, XXX–XXX

by the behavior of M' and M'' for a sample with 0.9 g of DNA/L (Figure 5). In an intermediate frequency range, M' and M'' run parallel and exhibit the characteristic $\omega^{1/4}$ scaling pertaining to Rouse dynamics. A fit of eq 14 to the parallel moduli gives the value of a. For concentrations exceeding 0.9 g of DNA/L, the time scaling exponent of the mean square displacement drops below the value pertaining to Rouse dynamics 1/4. The moduli M' and M'' are no longer parallel. Here, we have determined a by a fit of eq 14 to the data at the (single) frequency where $\langle \Delta x^2(t) \rangle$ and $M'(\omega)$ passes through $t^{1/4}$ and $\omega^{1/4}$ scaling, respectively. The optimized values of a are also shown in Figure 6B. The step length decreases from 0.26 μm to 45 nm when the concentration is increased from 0.2 to 1.5 g of DNA/L. If the entanglement correlation length is proportional to blob size ξ (constant number of entanglement strands per entanglement volume), the step length is predicted to follow $a \simeq c^{-0.77}$ scaling (Flory exponent $-\nu/(3\nu - 1)$ with $\nu = 0.588$).[22−24] The experimental results show a somewhat steeper decrease.

With the fitted values of the end-to-end distance R and step length a, the number of entanglements per chain can be calculated with $Z = R^2/a^2$. The results obtained from the diffusion experiments as well as those from previously reported microrheology experiments are displayed in Figure 7A (the

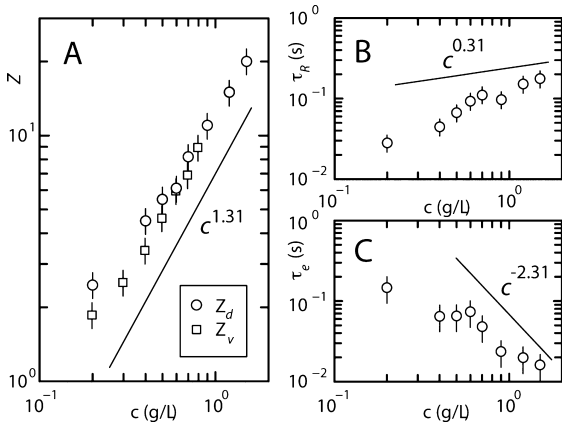

Figure 7. (A) Number of entanglements Z_d and Z_v, as obtained from diffusivity and viscoelasticity experiments, respectively, versus DNA concentration c. (B) As in panel A, but for the Rouse relaxation time τ_R. (C) As in panel A, but for the entanglement time τ_e. The solid lines represents the scaling laws for number of entanglements $Z \simeq c^{1.31}$, Rouse time $\tau_R \simeq c^{0.31}$, and entanglement time $\tau_e \simeq c^{-2.31}$.

viscosity data were obtained from 5/4 G/G_R with G and G_R the plateau and Rouse modulus, respectively[2,6]). Both data sets are in fair agreement. At low concentration Z is around unity. With increasing concentration, Z increases and follows the scaling law for an entangled polyelectrolyte with screened electrostatics $Z \simeq c^{1.31}$ (Flory exponent $1/(3\nu - 1)$ with $\nu = 0.588$).[22−24] At the highest concentration of 1.5 g of DNA/L, the number of entanglements per chain is around 20. For a sample of 2 g of λ-phage DNA/L, approximately 22 entanglements per chain has been reported in the literature based on bulk rheology measurements.[27]

The Rouse and entanglement times are related to the longest relaxation time and number of entanglements according to $\tau_R = \tau_d/(3Z)$ and $\tau_e = \pi^2\tau_d/Z^3$, respectively. Their values are displayed in Figure 7, parts B and C. To the best of our knowledge, the Rouse and entanglement times of reptating DNA have not been reported before. The experimental values of the Rouse time increase with increasing concentration and eventually take a value of around 0.2 s. Concomitantly, the entanglement time decreases from around 0.1 to 0.015 s. For a salted polyelectrolyte in the semidilute regime, the Rouse and entanglement time is predicted to follow $\tau \simeq c^{0.31}$ and $\tau \simeq c^{-2.31}$ scaling, respectively (Flory exponents $(2 - 3\nu)/(3\nu - 1)$ and $-3\nu/(3\nu - 1)$ with $\nu = 0.588$).[22−24] These scaling behaviors are indeed observed for concentrations exceeding 0.6 g of DNA/L, that is for concentrations well in the entangled regime.

Reorientational Dynamics. For the investigation of reorientational dynamics, we have uniformly labeled λ-phage DNA with YOYO-1. These labeled molecules are mixed with otherwise the same, but nonlabeled molecules and visualized with fluorescence microscopy. A series of images pertaining to a solution of 0.9 g of DNA/L is displayed in Figure 8A. For each

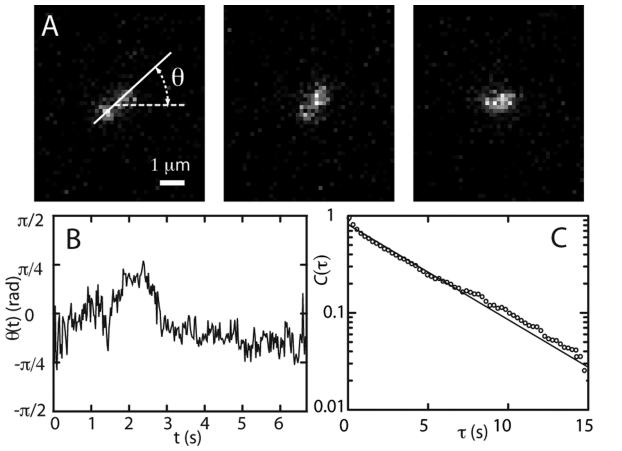

Figure 8. (A) Time sequence of a single YOYO-1 labeled DNA molecule immersed in a solution of 0.9 g of DNA/L and imaged with an interval of 5 s. The solid line represents the principal axis of the radius of gyration tensor. (B) Time evolution of the azimuthal angle $\theta(t)$ enclosed by the principal axis and the x-axis. (C) Autocorrelation of $\theta(t)$. The solid line represents a fit to an exponential.

frame, the radius of gyration tensor, that is principal values and orientation, was derived from the variation in fluorescence intensity. The radius of gyration tensor is slightly anisotropic with an time-averaged value $S_\perp/S_\parallel = 0.82 \pm 0.12$. The radius of gyration R_g of the entangled DNA molecules was obtained from the principal values according to eq 18. As discussed above, the values of R_g follow the relevant scaling law for a salted polyelectrolyte and are close to the values of the root-mean-square end-to-end distance R as derived from the analysis of the mean-square-displacement of the end-group (Figure 6B).

The anisotropy of the radius of gyration tensor is fairly constant, so that changes in tensor orientation are related to changes in molecular orientation rather than fluctuations in shape. The instantaneous orientation was obtained from the angle enclosed by the principal eigenvector and the x-axis according to eq 19. With increasing time, the molecule reorients with a concurrent change in orientation angle θ. Typical examples of the time evolution and autocorrelation of θ are shown in Figure 8, parts B and C, respectively. The autocorrelation function decays exponentially. Accordingly, eq 21 was fitted to the data by optimization of the reorientation time τ_r. The resulting reorientation times pertaining to different concentrations of DNA are also shown in Figure 6A. The

dx.doi.org/10.1021/ma501618a | Macromolecules XXXX, XXX, XXX−XXX

reorientation time τ_r is seen to increase by about an order of magnitude from 2.8 to 16 s once the concentration is increased from 0.7 to 1.7 g of DNA/L. We observe a quantitative agreement between τ_r and the tube renewal time τ_d. In particular, τ_r follows the same concentration scaling as the one for τ_d, that is $\tau_r \simeq c^{1.62}$. The quantitative agreement between the reorientation time and the tube renewal time shows that orientation correlation is lost once the molecule has diffused out of its original tube and has formed a new tube by tangling with other molecules.

CONCLUSIONS

We have obtained the lag-time dependent mean square displacement of quantum dot end-labeled λ-DNA. Because of long enough constraint release times at a concentration of 0.9 g of DNA/L, the entire sequence in time scaling from $t^{1/2}$, $t^{1/4}$, $t^{1/2}$, to t^1 with increasing lag-time t was observed. The mean square displacement was analyzed in the frequency domain in a similar way as in microrheology with particle video tracking. For this purpose, a complex diffusivity was calculated based on the one-sided Fourier transform of the mean square displacement. The complex diffusivity is similar in appearance as the viscoelastic moduli. This result is perhaps not unexpected because the dynamics of a tagged DNA molecule depends on viscoelastic dissipation in the surrounding fluid besides various internal relaxation modes. Advantages of our data analysis procedure are that differences in time scaling exponent translate into different, specific ratios of the real and imaginary parts of the complex diffusivity, clear indication of high frequency dispersion, and telltale crossover frequencies pertaining to the inverse longest relaxation time and entanglement time.

From a fit of the predictions of the Rouse model to the moduli in the low frequency range, we determined the longest relaxation time (tube renewal time) and end-to-end distance of the primitive path. The entanglement correlation length was determined from the characteristic $\omega^{1/4}$ scaling of the moduli pertaining to Rouse dynamics inside the tube at intermediate frequencies or the values of the moduli at the highest crossover frequency corresponding to the inverse entanglement time. Derived values of the longest relaxation times and number of entanglements per chain are in fair agreement with those obtained from microrheology. Furthermore, the observed concentration scaling of the longest relaxation time, number of entanglements, entanglement time, and Rouse relaxation time is in reasonable agreement with the relevant scaling laws predicted for salted polyelectrolytes with screened electrostatics. On the other hand, the end-to-end distance and entanglement correlation length show a rather steep decrease with increasing concentration of DNA. This effect might be related to well-known deficiencies of the Doi−Edwards theory in its present form, that is the neglect of contour length fluctuation and tube reorganization.

From imaging of uniformly labeled λ-DNA, we have also obtained the time-dependent orientation and principal values of the radius of gyration tensor. The time-averaged radius of gyration is in reasonable agreement with the end-to-end distance of the confinement tube as obtained from the analysis of the mean square displacement. Furthermore, the correlation time pertaining to reorientation of the radius of gyration tensor agrees with the tube renewal time as well as the longest relaxation time obtained from viscoelasticity experiments. The similarity in time scale for tube renewal and molecular reorientation brings unequivocally into view the coupled translational and reorientational motion of DNA molecules in the entangled regime.

AUTHOR INFORMATION

Corresponding Author

*(J.R.C.v.d.M.) E-mail: johanmaarel@gmail.com. Telephone: +65 65164396. Fax: +65 67776126.

Notes

The authors declare no competing financial interest.

ACKNOWLEDGMENTS

Patrick Doyle and Jeremy Jones are thanked for discussions and advice.

REFERENCES

(1) de Gennes, P. G. *J. Chem. Phys.* **1972**, *55*, 572.
(2) Doi, M.; Edwards, S. *The Theory of Polymer Dynamics*; Oxford University Press: New York, 1986.
(3) Perkins, T. T.; Smith, D. E.; Chu, S. *Science* **1994**, *264*, 819.
(4) Musti, R.; Sikorav, J.-L.; Lairez, D.; Jannink, G.; Adam, M. *C. R. Acad. Sci. Paris, Ser. IIb* **1995**, *320*, 599.
(5) Smith, D. E.; Perkins, T. T.; Chu, S. *Phys. Rev. Lett.* **1995**, *75*, 4146.
(6) Zhu, X.; Kundukad, B.; van der Maarel, J. R. C. *J. Chem. Phys.* **2008**, *129*, 185103.
(7) Kundukad, B.; van der Maarel, J. R. C. *Biophys. J.* **2010**, *99*, 1906.
(8) Kim, Y.; Kundukad, B.; Allahverdi, A.; Nordenskköld, L.; Doyle, P. S.; van der Maarel, J. R. C. *Soft Matter* **2013**, *9*, 1656.
(9) Kremer, K.; Grest, G. S.; Carmesin, I. *Phys. Rev. Lett.* **1988**, *61*, 566.
(10) Smith, G. D.; Paul, W.; Monkenbusch, M.; Richter, D. *Chem. Phys.* **2000**, *261*, 61.
(11) Larson, R. G. *J. Polym. Sci., Part B: Polym. Phys.* **2007**, *45*, 3240.
(12) Putz, M.; Kremer, K.; Grest, G. S. *Europhys. Lett.* **2000**, *49*, 735.
(13) Uneyama, T.; Akimoto, T.; Miyaguchi, T. *J. Chem. Phys.* **2012**, *137*, 114903.
(14) Komlosh, M. E.; Callaghan, P. T. *J. Chem. Phys.* **1998**, *109*, 10053.
(15) Herrmann, A.; Kresse, B.; Wohlfahrt, M.; Bauer, I.; Privalov, A. F.; Kruk, D.; Fatkullin, N.; Fujara, F.; Rossler, E. A. *Macromolecules* **2012**, *45*, 6516.
(16) Mason, T. G.; Ganesan, K.; van Zanten, J. H.; Wirtz, D.; Kuo, S. C. *Phys. Rev. Lett.* **1997**, *79*, 3282.
(17) Mason, T. G.; Dhopple, A.; Wirtz, D. *Macromolecules* **1998**, *31*, 3600.
(18) Mason, T. G. *Rheol. Acta* **2000**, *39*, 371.
(19) Chen, D. T.; Weeks, E. R.; Crocker, J. C.; Islam, M. F.; Verma, R.; Gruber, J.; Levine, A. J.; Lubensky, T. C.; Yodh, A. G. *Phys. Rev. Lett.* **2003**, *90*, 108301.
(20) Savin, T.; Doyle, P. S. *Biophys. J.* **2005**, *88*, 623.
(21) Hsieh, C. C.; Balducci, A.; Doyle, P. S. *Macromolecules* **2007**, *40*, 5196.
(22) de Gennes, P.-G. *Scaling Concepts in Polymer Physics*; Cornell University Press: Ithaca, NY, 1979.
(23) Teraoka, I. *Polymer Solutions: An Introduction to Physical Properties*; John Wiley & Sons: New York, 2002.
(24) van der Maarel, J. R. C. *Introduction to Biopolymer Physics*; World Scientific: Singapore, 2008.
(25) Nepal, M.; Yaniv, A.; Shafran, E.; Krichevsky, O. *J. Chem. Phys.* **2013**, *110*, 058102.
(26) Verma, R.; Crocker, J. C.; Lubensky, T. C.; Yodh, A. G. *Phys. Rev. Lett.* **1998**, *81*, 4004.
(27) Teixeira, R. E.; Dambal, A. K.; Richter, D. H.; Shaqfeh, E. S. G.; Chu, S. *Macromolecules* **2007**, *40*, 2461.
(28) http://physics.georgetown.edu/matlab/.